PRINTABLE EPOXY CARBON FIBER COMPOSITES AND THEIR MECHANICAL PROPERTIES

Andrew Abbott[1,3], Emrah Celik[1,2], Harry A. Pierson[1,4], Hilmar Koerner[1], Jeffery W. Baur[1]

[1] Air Force Research Laboratory, Wright Patterson Air Force Base, OH

[2] University of Dayton Research Institute, Dayton, OH

[3] Department of Aerospace and Mechanical Engineering, University of Miami, Miami, FL

[4] Department of Industrial Engineering, University of Arkansas Fayetteville, AR

ABSTRACT

Additive manufacturing (AM) of fiber reinforced thermosetting resins has not been well explored due to material and processing restrictions including high viscosity, poor reinforcement dispersion, dimensional tolerance, and porosity. Yet, such a process would enable tool-less and agile manufacturing of small and complex composite parts with temperature and environmental stability superior to traditional thermoplastics. Printed thermoset composites could also be combined with traditional epoxy prepregs to make complex co-cured structures. In this work, a direct write AM process for epoxy / chopped carbon fiber composites is used which has been shown to provide cured composites tensile modulus and strength values 90% and 66% of the fully aligned composite, respectively. The fibers are largely oriented in the print direction, but have sufficient localized material flow to achieve acceptable transverse properties and low porosity. Sandwich structures created with additively printed cores and co-cured prepreg face sheets were fabricated and evaluated. Rather than creating a sandwich structure by adhesively bonding standard sizes of honeycomb core to cured composite face sheets, this work examined co-curing customized additively printed core structures with prepreg face sheets. This process can be used to design and optimize properties for complex geometries while reducing the number of manufacturing steps.

1. INTRODUCTION

1.1 Background

Additive manufacturing (AM) is a rapidly maturing manufacturing process driven by advantages in achieving complex geometries from digital representations, tool-less fabrication, short lead times, and the potential for low-quantity production [1]. To benefit from these advantages, industries are maturing AM processes from prototyping applications to load-bearing structural applications. While metal AM technology is currently leading the charge, there is an appetite for AM of structural polymer matrix composites. Several polymer AM techniques have been explored for fabrication of composite materials. Fused filament fabrication is a melt extrusion process in which a thermoplastic polymer filament is melted, extruded through a nozzle, and built up layer-by-layer. It has been used to print a number of thermoplastics reinforced with several fillers including glass, carbon, and Kevlar fiber [2-7], as well as metal and nanoparticles [8-11] which improved tensile and bending properties. However, these composites often retain the low service temperature of the resin and suffer from high porosity, sub-optimal bonding between roads/layers, and less than desirable environmental durability. Stereolithography has been used to photocure filled UV-curable materials [12-16], but these systems are limited by filler optical absorbance and scattering which restricts the type and amount of filler that can be added.

Recently, thermosetting resins have been printed with short-fiber reinforcement that maintain their printed shape throughout a cure cycle [17]. In comparison to the large amount of studies on thermoplastic polymers, AM thermosetting polymers and their composites offer the potential to address many of the above-mentioned limitations. Thermosetting materials common to many aerospace applications may also be used. Rather than melting, a direct write process deposits a fluid with sufficient yield stress to form self-supporting structures. The high yield stress can be achieved by using rheological modifiers such as nanoclay. In this manner, the entire printed structure can be printed at room-temperature and cured in a secondary process. The room temperature printing significantly reduces the dependence of the mechanical properties on thermal printing history and location that is often encountered in melt-based filament-based AM methods.

1.2 Overview

The direct write method has been previously applied to the fabrication of silicon carbide, chopped carbon fiber, and nanoclay reinforced thermosets [17,18]. Recently, inks consisting of epoxy resin, a latent cure agent, nanoclay rheological modifiers, and chopped carbon fiber reinforcement have been printed at modest fiber volume loadings to achieve strength and stiffness values approaching those of the fully aligned chopped fiber composite. Additionally, processing variations which produce helically oriented fibers have shown to achieve improved damage resistance [19]. The previous study explored process parameters including fiber length, fiber loading, and fiber orientation on the mechanical performance of additively manufactured thermoset composites and compared them to compression molded specimens [20]. Within this paper, we summarize the application of this previous work and extend it to create hybrid processed sandwich structures in which the complex shaped sandwich core is additively printed and traditional prepreg sheets of uniaxial carbon fiber epoxy sheets are used as face sheets. The complete structure is oven co-cured and then tested in bending.

2. EXPERIMENTATION

2.1 Ink Formulation and Processing

Chopped carbon fiber filled epoxy inks consisted of EPON 826 epoxy from Hexion, Inc, Garamite 7305 clay from BYK Additives, chopped standard modulus fiber with epoxy sizing from Hexcel, and a latent ionic liquid curing agent 1-ethyl-3-methylimidazolium dicyanamide from Sigma-Aldrich. Garamite 7305 is a mixture of sepiolite and montmorillonite clays which serves as a rheology modifier imparting the ink with shear-thinning character and a yield stress. The chopped carbon fiber comes as 6 mm long tape segments each comprised of 5 μm diameter filaments held together by sizing. The ionic liquid curing reacts very slowly at room temperature allowing for a working time of several days. At temperatures above about 80°C, the reaction kinetics increase dramatically and full cure is attained in a matter of hours. The reaction mechanism is not stoichiometric, and therefore a high degree of cure is achieved with only small quantities of curing agent. This is beneficial because typical epoxy curing agents are low viscosity liquids which act as diluents which increase the mass of rheology modifier required to generate a yield stress fluid.

Garamite 7305 clay was added stepwise into EPON 826 epoxy resin to a total ratio of 10 parts per hundred (pph) with respect to epoxy. After each step (5 total), it is mixed in a Thinky ARV-310 planetary mixer for 1 min at 2,000 rpm. Next, the chopped carbon fiber is added in 5 steps and mixed for 1 min at 2,000 rpm after each addition. Once the fiber tape is reasonably separated into individual filaments in the epoxy/clay mixture, it is mixed under vacuum for 9 min total in 3 min intervals at 2,000 rpm to both disperse and fracture fibers. Mixing ink containing fibers generates significant heat which reduces resin viscosity hindering fiber breakage. Therefore, mixing is conducted in 3 min increments, and the ink is allowed to cool before conducting the next mixing step. After the fibers are mixed into the ink and their lengths reduced, the curing agent is added and mixed under vacuum for 1 min at 2,000 rpm.

The main ink used in this study had a fiber loading of 5.5 vol%. This carbon fiber loading was selected because it was found to yield an optimal balance between fiber loading and fiber length. As loading increased, the high shear mixing decreased the average fiber length and a knockdown in mechanical properties was observed. Above a fiber loading of 5.5 vol%, mechanical properties began to decrease.

2.2 Printing Procedure

Direct ink printing was performed on an nScrypt 3Dn-500 system. The system is equipped with a 3-axis Aerotech gantry controllable with Gcode. Ink was extruded out of 0.58 mm diameter dispense nozzles connected to 10 cm^3 syringes with pressure applied by a piston powered by compressed nitrogen and controlled by a pressure pump. A Nordson Ultimus V pressure pump was used to programmatically set pressure and toggle pressure on/off. Mixed ink was loaded into 10 cm^3 syringes with a spatula. Air entrapped during the syringe loading process was removed by centrifuging the syringes at 4,000 rpm for 20 min. A 0.58 mm inner diameter tapered polypropylene dispense nozzle was connected via luer-lok to each syringe. Syringes were then placed into a 10 cm^3 high pressure adapter which amplified the pressure by a factor of about 3.

Print parameter calibrations were performed by first extruding ink at a sufficient pressure to ensure a uniform flowrate. Next, ink was extruded for 3 seconds and the extrudate mass was measured to calculate the mass flow rate. Mass flow rate was divided by an approximate ink density (1.22 g/cm^3) to give a volumetric flow rate. Dividing the volumetric flow rate by the cross-sectional area of the dispense nozzle yielded a linear flow rate which was taken as the print speed. Road width was taken to be equal to 0.5 mm. For printed tensile and flexure coupons, the layer height was also taken to be 0.5 mm. Other sets were printed to test various layups for directional properties with different infill orientations and to understand how localized transverse flow helps to reduce the porosity. These included transverse $[90°]_s$, $[0°/\pm45°/90°]_s$ quasi-isotropic, and $[\pm45°]_{2s}$ cross hatch laminates. For printed hexagonal cores, the layer height was determined by measuring the height of a single printed line using a Keyence optical profilometer.

2.3 Mechanical Testing of Printed Inks

2.3.1 Tensile testing

Uniaxial tensile test coupon dimensions followed those specified for type V coupons in ASTM standard D638. Testing was performed on an MTS Insight screw-driven system with a 30 kN load cell at a displacement rate of 1 mm/min. Digital image correlation (DIC) was used to measure true strain during tensile testing. Coupons were speckled with white paint, and a CCD camera captured images of coupons during testing at a rate of 2 Hz. Speckle positions were tracked image-to-image using VIC-2D software generating true strain data. At least 5 coupons were tested for each ink formulation.

2.3.2 Flexure testing

Flexure tests were performed in the 3-point bending configuration on a Tinius Olsen H10KS. Coupons were 150 x 12.7 mm following ASTM D7264 with a height ranging from 2.4 to 3 mm. The support span was adjusted based on individual coupon thickness to maintain a span-to-thickness ratio of 20:1. The crosshead was displaced at a rate of 6 mm/min. Strain was calculated from crosshead displacement and stress calculated from applied force and coupon dimensions.

2.4 Sandwich Structure Fabrication

2.4.1 Prepreg layup and printing

Composite sandwich structures were fabricated with unidirectional 5320/T40 800B prepreg for the face sheets and 5.5 vol% (10 pph) carbon fiber ink to print the core. First, prepreg was cut to 101.6 mm (4 in) by 38.1 mm (1.5 in) with the 4 in direction parallel to the fiber axis. Next, 4 plies were pressed together by hand with a wooden dowel. Then, the 4 ply layup was placed on double-sided polyimide tape on a borosilicate glass plate. Three hexagonal core structures were printed with different fill densities which were controlled by changing the hexagon edge lengths. The 3 edge lengths used were 5, 10, and 15 mm which corresponded to area fraction of approximately 12, 7, and 5% respectively. The target core thickness was 7.62 mm (0.3 in). After printing the core, another 4 ply face sheet was carefully placed on top of the core and gently tapped down onto the core in an attempt to increase the contact area. Sandwich structures were cured freestanding at 121 °C for 2 hr followed by 177 °C for 2 hr.

2.4.2 Flexure testing sandwich structures

Preliminary 3-point flexure tests were performed on an MTS Insight 30 SL load frame outfitted with a 30 kN load cell. The crosshead displacement rate was 6 mm/min. Specimen dimensions were based on ASTM C393 and scaled by a factor of 0.5. The support span was 76.2 mm (3 in). All tests were performed at room temperature.

2.4.3 Adhesion improvement techniques

Techniques were explored to improve adhesion between the printed core and the top face sheet. The first technique was to add weight onto the structure to press the top face sheet into the printed core. Although some deformation was expected in the core, it was primarily expected to occur where the contact area was low and therefore pressure high, thereby flattening the rough surface of the printed core. The second technique was to smooth the core surface by wiping with a straight, flat blade prior to placing the prepreg face sheet.

For the first technique, a rigid, transparent plastic was substituted for the face sheets so that the contact between the core and the face sheets could be qualitatively assessed. After printing the core and placing the top face sheet, the sandwich structure was flipped over for 5 minutes and then inspected for improvements in contact area. Glass slides weighing 9.5 g were added on top of the structure incrementally. After 5 minutes, the slides were removed and the contact area was examined before adding the next slide.

For the second technique, a razor blade was mounted onto the Aerotech gantry and translated across the top of the core at a rate of 10 mm/s for about 20 passes lowering by 10 µm after each pass. The blade was positioned to touch only the highest points on the core's rough surface on the first pass to minimize the amount of material that was smoothed on each pass.

3. RESULTS

3.1 Mechanical Properties of Printed Coupons

3.1.1 Mechanical testing results – flexure

Mechanical test results for both compression molded and printed coupons tested in flexure are summarized in Figure 1. Longitudinal refers to coupons in which the printing direction is along the longitudinal axis of the coupon; a 0° infill orientation. Random (CM) refers to compression molded coupons in which the fiber orientation is in-plane random without preferential axial or transverse alignment. Transverse refers to coupons which were printed with the infill direction orthogonal to the longitudinal direction; a 90° infill orientation. As seen in Figure 1, coupons printed longitudinally yielded the greatest flexure strength and modulus with a 33% increase in strength and 52% increase in modulus over CM coupons. Transversely printed coupons saw a 37% and 21% knockdown in strength and modulus respectively compared to CM coupons. These results demonstrate the freedom that printing provides to tune directional mechanical properties.

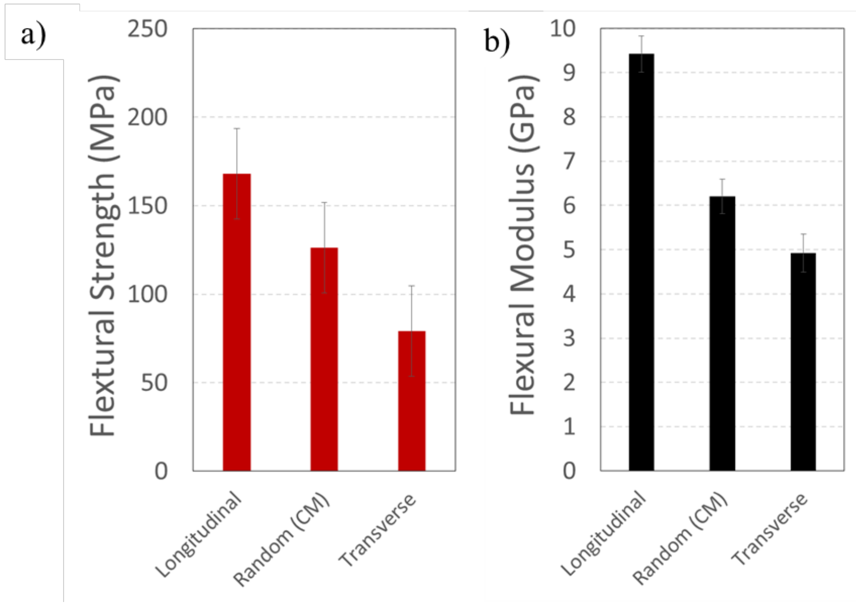

Figure 1. Influence of fabrication method on (a) flexure strength and (b) flexure modulus of compression molded (CM) and longitudinally and transversely printed test specimens.

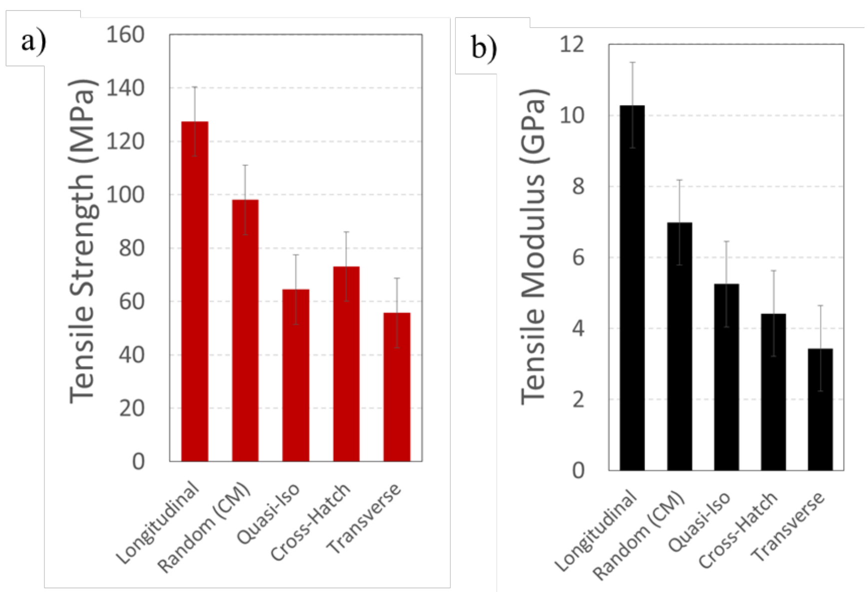

Figure 2. Influence of processing method and print direction on (a) tensile strength and (b) tensile modulus of compression molded, longitudinal [0], transverse [90],, quasi-iso $[0/\pm45/90]_s$, and cross-hatch $[\pm45]_{2s}$ specimens.

Tensile strength and modulus of CM coupons and printed laminates are summarized in Figure 2. Quasi-iso and cross-hatch refer to quasi-isotropic and ±45° laminates, respectively. As with the flexure coupons, the longitudinal print direction yielded the highest strength and modulus and the transverse print direction yielded the lowest values, as expected. Longitudinal tensile strength and modulus were 30% and 47% greater than CM, respectively. Unexpectedly, quasi-isotropic and cross-hatch coupons yielded lower tensile properties than CM coupons. This reduction is attributed to rough as-printed surfaces with sites of stress concentrations. Quasi-isotropic and cross-hatch top surfaces were not machined because material removal would either reduce the top layer thickness or completely remove the top layer leaving an unbalanced laminate. Transverse tensile strength and modulus were 43% and 51% less than CM, respectively. Again, these data show control over mechanical properties by manipulating the print direction.

Increased mechanical properties in longitudinally printed coupons compared to compression molded coupons are attributed to fiber orientation resulting from shear-induced alignment in the extrusion process. Fiber alignment also explains the reduction in transverse properties compared to CM. SEM images of fracture surfaces of printed and CM coupons in Figure 3 show the difference in fiber alignment. Fracture surfaces of a CM coupon in Figure 3a and Figure 3b show a lack of alignment in any specific direction. The fiber axes are random in-plane. In contrast, Figure 3c and Figure 3d show fracture surfaces of a printed coupon with good fiber alignment. In this longitudinally printed coupon, the fibers are primarily aligned normal to the fracture surfaces.

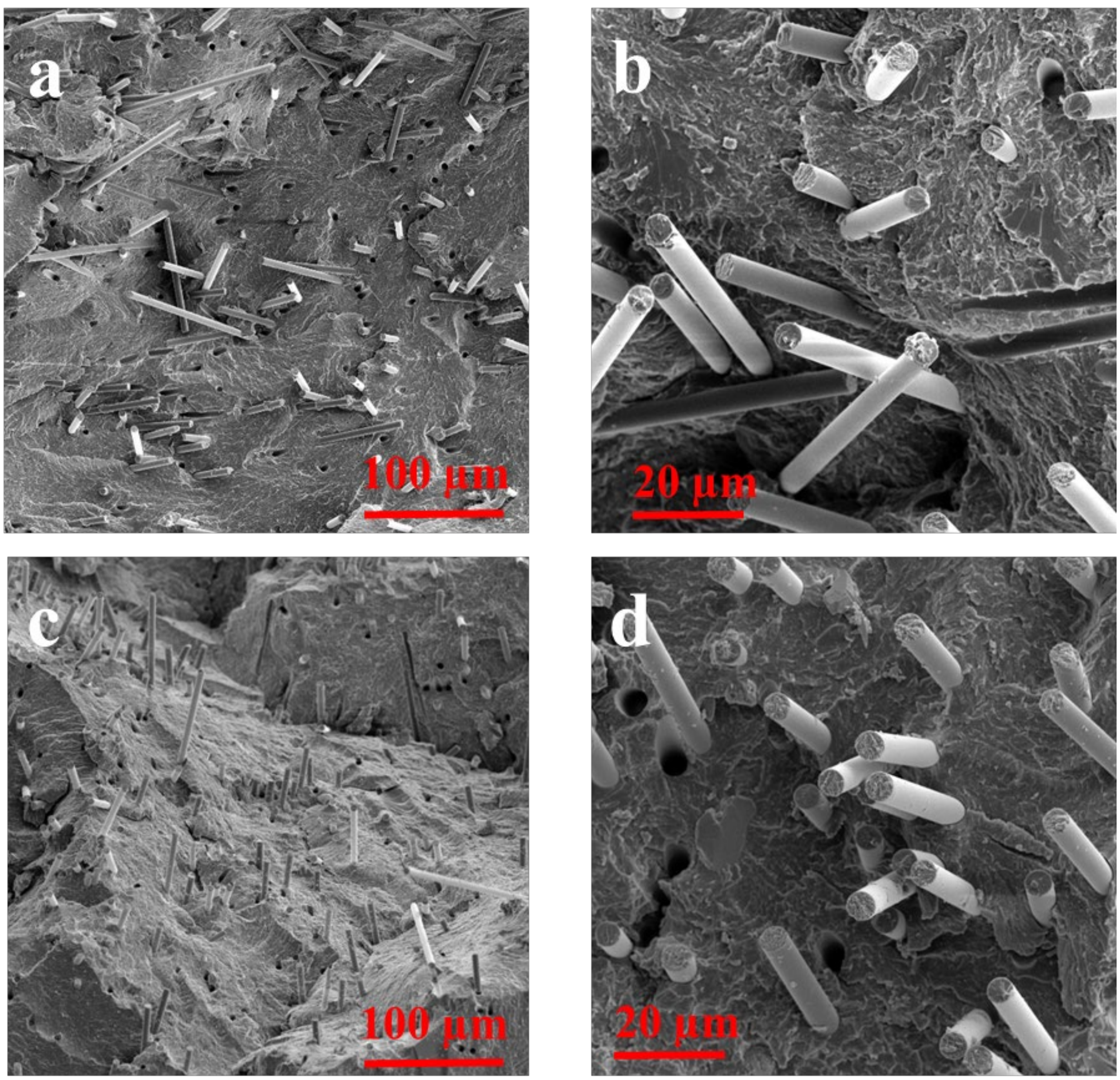

Figure 3. Fiber alignment from SEM images of compression molded, (a) and (b), and printed, (c) and (d), fracture surfaces.

The degree of fiber alignment in printed coupons was approximated by calculating Herman's orientation parameter from Fourier transforms of x-ray computed tomography (CT) images. Through thickness image slices were captured for a printed and cured 10 pph carbon fiber tensile coupon using x-ray CT. Select images were fast Fourier transformed in ImageJ. Azimuthal integration of the resulting images was performed using Fit2D. After background subtraction, Herman's orientation parameter was calculated. Herman's orientation parameter ranges from -0.5 (transverse alignment) to 0 (random alignment) to 1 (perfect alignment in the printing direction). The calculated value was 0.6 indicating good fiber alignment in the printing direction, but with room for improvement.

Additionally, the cross-section of the alternating 2-layer crosshatch pattern (±45°) and an 8-layer symmetric quasi-isotropic pattern (0°, 45°, -45°, 90°) shown in Figure 4 further demonstrates fiber orientation programmability. While these layered materials had lower mechanical properties than the compression molded specimens due to surface defects, they had low internal porosity. Overall, the density of the AM structures were measured to be within 1% of compression molded samples [20].

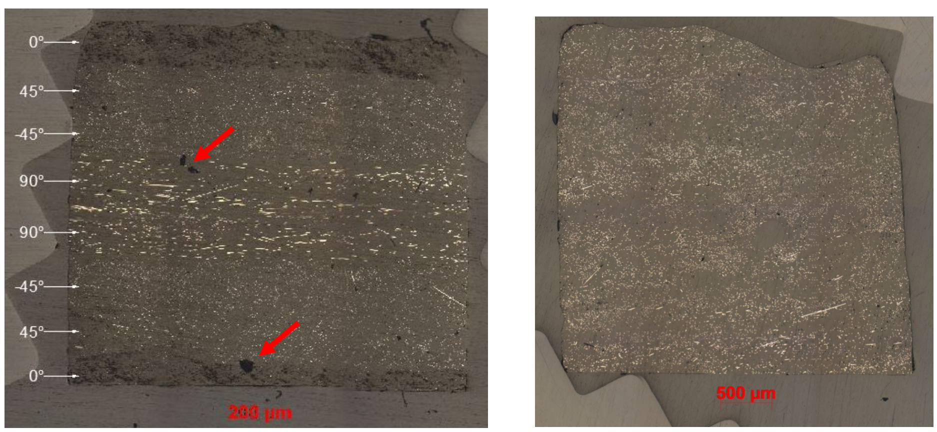

(a) (b)

Figure 4. Optical microscopy of polished cross sections for (a) quasi-isotropic and (b) crosshatch 10 pph CF samples. Arrows indicate porosity caused by bubbles entrapped in the ink during syringe loading [20].

3.2 Sandwich structures

3.2.1 Sandwich structure fabrication challenges

One key challenge encountered with printing sandwich cores was related to flow of the extruded ink and wall thinness. Because the walls of the hexagonal patterns were only a single road wide, the ink was free to flow laterally more than when printing a fully dense layer comprised of several adjacent roads. Lateral flow complicated print parameter calibration because layer heights were inconsistent through the thickness. Measuring layer height of a single road and using that value to print a stack of five roads did not yield a total height equal to five layer heights, but rather a smaller total height. Updating the layer height to that of the average layer height from the five road stack height and printing additional layers yielded still a smaller average layer height values. Print speed, pressure, and occasionally first layer offset distance were adjusted until a more consistent layer height was obtained. Even after careful calibration, printed cores were only about 6 mm thick compared to the targeted 7.62 mm. This thickness corresponded to 30-40 printed layers. Any small error in individual layer height was compounded with each subsequent layer which caused the distance between the nozzle and the previous layer to increase throughout the print. In some cases, the nozzle was over 0.5 mm from the previous layer by the end of the print, causing flow instabilities manifesting as non-straight, snaking roads. In extreme cases, roads were partially deposited off the previous layer and down the wall. Careful print parameter calibration reduced, but did not eliminate, this problem.

3.2.2 Sandwich structure flexure testing

The high yield stress of the ink enabled placement of top face sheets without noticeable sagging or deformation of the core. All sandwiches survived the cure cycle without any core collapse. Two coupons were made for each of the three hexagon sizes. It was expected that the interface between the top face sheet and core would be weaker than between the bottom face sheet and the core due to the difference in pressure from the weight of the core material. Therefore, flexural testing was performed with the top face sheet on the bottom in tension and expected to lead to failure at lower deflection. In this way, the minimum failure strength is obtained and a baseline for comparison to future tests is provided.

Select results are presented in Figure 5. The number indicates the calculated core shear stress at the maximum load. As expected, the highest fill density featured the highest peak load. Oddly, the 15 mm hexagon edge length had a higher peak load than the 10 mm edge length. This is attributed to insufficient contact between the core and top face sheet caused by uneven printed surfaces. All face sheets were lightly tamped down onto the core by hand. A better method of applying repeatable load to top face sheets should be explored. Fracture progressed in 2 modes shown in Figure 6. First, debonding between the core and top face sheet progressed incrementally with each debond accompanied by a drop in load. Abrupt failure occurred as a result of shear failure in the core. All tests were stopped after core failure. Improving the face sheet-core bond strength via smoother printed surfaces or more uniform and repeatable compaction is expected to yield higher peak loads. Overall, peak shear stress in the core is low, but must be compared to literature values for typical epoxies.

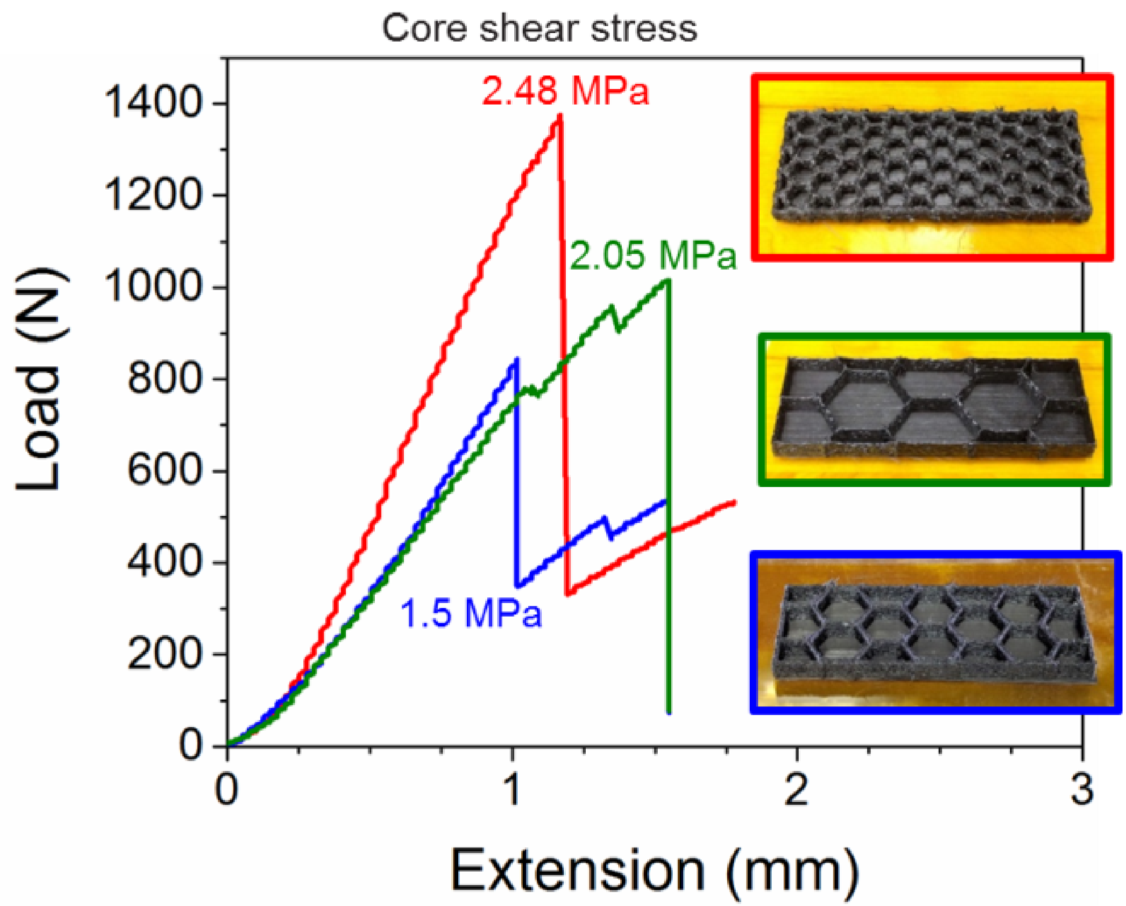

Figure 5. Hybrid sandwich structure flexure results for printed core with edge lengths of 5 mm (outlined in red at the top), 10 mm (outlined in blue at the bottom), and 15 mm (outlined in green in middle) corresponding to area fractions of 12%, 7%, and 5%, respectively.

Figure 6. Typical failure mode of debonding between top face sheet and core followed by shear failure of the printed core.

3.2.3 Preliminary results of adhesion improvement techniques

The first technique of flipping a sandwich structure onto the top face sheet and then adding weight in the form of glass slides ultimately increased the contact between the face sheet and the core, but at the expense of core deformation. Figure 7 shows the progression of contact area improvement as weight was added. Flipping the sandwich structure onto the top face sheet for five minutes without the application of any additional weight did not make a perceptible difference in the contact area (Figure 7a). After the first 9.5 g glass slide was added, improvements in the contact area were observed only at the highest points of the core's rough top surface. Further improvements to contact area were observed with each successive addition of a glass slide. However, after the third slide, deformation was observed in the core, and the ink began to flow beyond the edges of the face sheets. After the fifth glass slide (Figure 7c), the contact area had improved substantially, but the core was further compressed.

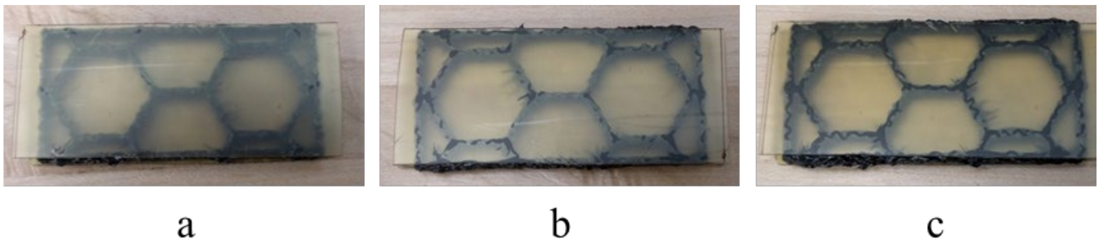

Figure 7. Progression of core/top face sheet contact area (a) before applying addition weight, (b) after adding weight of 2 glass slides for 5 min, and (c) after 5 glass slides.

The second technique by which a straight edge was rastered over the printed core and lowered 10 μm after each pass demonstrated sufficiently improved contact area compared to the first technique. The printed core is shown in 8a after smoothing and the contact area is shown in 8b. The primary concern with this technique is the resulting shear deformation. To limit total shear deformation of the ink, the straight edge was rastered in a back-and-forth motion. Because the ink is shear thinning, viscosity decreases with increasing shear rate allowing the ink to flow. To avoid too much ink flow, the straight edge translation rate, and therefore shear rate, was slow. Given the thickness of the core and the translation rate, the approximate shear rate is 1.7 s^{-1}.

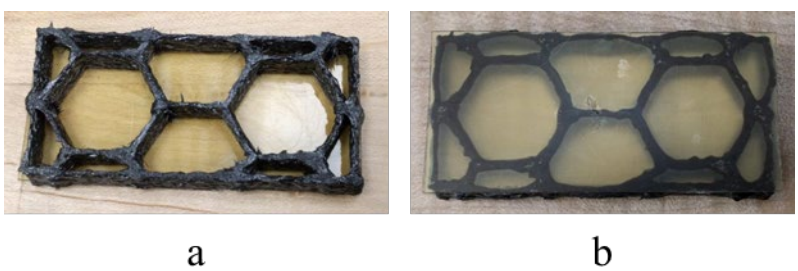

Figure 8. Printed core structures on transparent face sheets (a) after smoothing (no top face sheet) and (b) core contact area with top face sheet.

At this time, mechanical testing of sandwich specimens with smoothed cores has not been completed. The increased core flatness and bond area are expected to lead to higher peak flexural loads. If not observed, several alternative approaches are being considered. However, these approaches may reduce the processing simplicity of the current process and the perceived mechanical advantages in co-curing the sandwich constituents.

4. CONCLUSIONS

This research demonstrated an AM process for epoxy matrix chopped carbon fiber composites that has the potential to improve tensile and flexural properties, temperature capability, and environmental durability over common polymer filament-based AM methods. Imaging of the ink confirmed good fiber alignment of carbon fiber in the print direction as induced by shear stresses during the extrusion process. Experimental mechanical results are consistent with high alignment in the print direction and the localized transverse flow which together create composites with tailored reinforcement, low porosity, and desirable mechanical properties. As expected due to the fiber orientation in the print direction, longitudinal printed laminates had higher tensile and flexural properties than compression molded (CM) specimens and laminates tested transverse to the print direction had properties lower than the CM specimens. Quasi-isotropic and cross-hatched layer ink laminates were also demonstrated. Because the surface of these specimens were not machined to remove defects, their mechanical properties were lower than the CM specimens.

The printing of thermosetting reinforced ink was also extended to hexagonal sandwich core structures of different sizes with co-cured uniaxial face sheets. When the sandwich panels were tested in flexure, they tended to first debond between the top face sheet and the printed core and then fail in shear within the core. Techniques to improve the core/face sheet contact area were investigated and appear promising. Further testing of their effects on interfacial strength is underway. Overall, the hybrid manufacturing of co-cured sandwich panels with spatially varying core structures has advantages for tailoring mechanical properties to the specific application, as well as decreasing production time and costs.

5. ACKNOWLEDGEMENTS

The authors would like to thank Hugh De Jarnette, Leonardo Sierra Gutierrez, and Kyle Johnson for their technical assistance. The authors would also like to thanks the AFRL Summer Faculty program and the AFRL International Cooperative Research & Development Fund for financial support.

6. REFERENCES

1. Groover, M. P. *Fundamentals of Modern Manufacturing: Materials, Processes, and Systems*. 6th edn. USA: Wiley, 2015
2. Brenken, B., Barocio, E., Favaloro, A., Kunc, V., Pipes, R. B. "Fused filament fabrication of fiber-reinforced polymers: A review." *Additive Manufacturing* 21 (2018): 1-16. https://doi.org/10.1016/j.addma.2018.01.002
3. Ning, F., Cong, W., Qiu, J., Wei, J., Wang, S. "Additive manufacturing of carbon fiber reinforced thermoplastic composites using fused deposition modeling." *Composites Part B: Engineering* 80 (2015): 369-378. https://doi.org/10.1016/j.compositesb.2015.06.013
4. Araya-Calvo, M., López-Gómez, I., Chamberlain-Simon, N., León-Salazar, J. L., Guillén-Girón, T., Corrales-Cordero, J. S., Sánchez-Brenes, O. "Evaluation of compressive and flexural properties of continuous fiber fabrication additive manufacturing technology." *Additive Manufacturing* 22 (2018): 157-164. https://doi.org/10.1016/j.addma.2018.05.007

5. Blok, L. G., Longana, M. L., Yu, H., Woods, B. K. S. "An investigation into 3D printing of fibre reinforced thermoplastic composites." *Additive Manufacturing* 22 (2018): 176-186. https://doi.org/10.1016/j.addma.2018.04.039
6. Zhong, W., Li, F., Zhang, Z., Song, L., Li, Z. "Short fiber reinforced composites for fused deposition modeling." *Materials Science and Engineering: A* 301 (2) (2001): 125-130. https://doi.org/10.1016/S0921-5093(00)01810-4
7. Quan, Z., Larimore, Z., Wu, A., Yu, J., Qin, X., Mirotznik, M., Suhr, J., Byun, J.-H., Oh, Y., Chou, T.-W. "Microstructural design and additive manufacturing and characterization of 3D orthogonal short carbon fiber/acrylonitrile-butadiene-styrene preform and composite." *Composites Science and Technology* 126 (2016): 139-148. https://doi.org/10.1016/j.compscitech.2016.02.021
8. Nikzad, M., Masood, S. H., Sbarski, I. "Thermo-mechanical properties of a highly filled polymeric composites for Fused Deposition Modeling." *Materials & Design* 32 (6) (2011): 3448-3456. https://doi.org/10.1016/j.matdes.2011.01.056
9. Shofner, M. L., Lozano, K., Rodríguez-Macías, F. J., Barrera, E. V. "Nanofiber-reinforced polymers prepared by fused deposition modeling." *Journal of Applied Polymer Science* 89 (11) (2003): 3081-3090. https://doi.org/10.1002/app.12496
10. Skorski, M. R., Esenther, J. M., Ahmed, Z., Miller, A. E., Hartings, M. R. "The chemical, mechanical, and physical properties of 3D printed materials composed of TiO2-ABS nanocomposites AU - Skorski, Matthew R." *Science and Technology of Advanced Materials* 17 (1) (2016): 89-97. https://doi.org/10.1080/14686996.2016.1152879
11. Jakus, A. E., Taylor, S. L., Geisendorfer, N. R., Dunand, D. C., Shah, R. N. "Metallic Architectures from 3D-Printed Powder-Based Liquid Inks." *Advanced Functional Materials* 25 (45) (2015): 6985-6995. https://doi.org/10.1002/adfm.201503921
12. Martin, J. J., Fiore, B. E., Erb, R. M. "Designing bioinspired composite reinforcement architectures via 3D magnetic printing." *Nature Communications* 6 (2015): 8641. https://doi.org/10.1038/ncomms9641
13. Kim, K., Zhu, W., Qu, X., Aaronson, C., McCall, W. R., Chen, S., Sirbuly, D. J. "3D Optical Printing of Piezoelectric Nanoparticle–Polymer Composite Materials." *ACS Nano* 8 (10) (2014): 9799-9806. https://doi.org/10.1021/nn503268f
14. Yugang, D., Yiping, T., Yuan, Z., Dichen, L. "Nano-TiO2-modified photosensitive resin for RP." *Rapid Prototyping Journal* 17 (4) (2011): 247-252. https://doi.org/10.1108/13552541111138360
15. Hector Sandoval, J., Wicker, R. B. "Functionalizing stereolithography resins: effects of dispersed multi-walled carbon nanotubes on physical properties." *Rapid Prototyping Journal* 12 (5) (2006): 292-303. https://doi.org/10.1108/13552540610707059
16. Lin, D., Jin, S., Zhang, F., Wang, C., Wang, Y., Zhou, C., Cheng, G. J. "3D stereolithography printing of graphene oxide reinforced complex architectures." *Nanotechnology* 26 (43) (2015): 434003. https://doi.org/10.1088/0957-4484/26/43/434003
17. Compton, B. G., Lewis, J. A. "3D-printing of lightweight cellular composites." *Adv Mater* 26 (34) (2014): 5930-5935. 10.1002/adma.201401804
18. Hmeidat, N. S., Kemp, J. W., Compton, B. G. "High-strength epoxy nanocomposites for 3D printing." *Composites Science and Technology* 160 (2018): 9-20. https://doi.org/10.1016/j.compscitech.2018.03.008

19. Raney, J. R., Compton, B. G., Mueller, J., Ober, T. J., Shea, K., Lewis, J. A. "Rotational 3D printing of damage-tolerant composites with programmable mechanics." *Proceedings of the National Academy of Sciences* 115 (6) (2018): 1198. https://doi.org/10.1073/pnas.1715157115
20. Pierson, H. A., Celik, E., Abbott, A., De Jarnette, H., Sierra Gutierrez, L., Johnson, K., Koerner, H., Baur, J. "Mechanical Properties of Printed Epoxy-Carbon Fiber Composites." *Manuscript submitted for publication* (2018):